

Superposition model of mode shapes composed of travelling torsional guided waves excited by multiple circular transducer arrays in pipes

Xudong Niu^{a,b,c}, Kong Fah Tee^{b,*}, Hugo R. Marques^d

^a NSIRC, TWI Ltd, Granta Park, Cambridge CB21 6AL, UK.

^b School of Engineering, University of Greenwich, Central Avenue, Kent ME4 4TB, UK.

^c Department of Mechanical Engineering, University of Bristol, University Walk, Bristol BS8 1TR, UK.

^d TWI Ltd, Granta Park, Cambridge CB21 6AL, UK.

* Corresponding author. E-mail address: K.F.Tee@gre.ac.uk

Abstract

In pipe inspection using ultrasonic guided wave technique, the current commercial transmitters are designed for the unidirectional guided wave excitation using multiple circular piezoelectric transducers arrays in the axial direction. However, the source with many individual transducer elements in arrays has difficulty in achieving an axisymmetric loading perfectly for defect detection. Therefore, a quasi-axisymmetric wave is formed due to many undesired wave modes are launched instead of a pure axisymmetric wave at a given excitation frequency. In this paper, a realistic superposition model of axial multiple transducer arrays is proposed. The model has many potential applications; one example is investigating the source influence on the generated quasi-axisymmetric wave effect. The analytical model is employed to achieve the predictions for investigating a transmitter's influence for the unidirectional enhancement of torsional $T(0,1)$ guided wave mode excitation in a pipe inspection system composing of three piezoelectric transducer ring arrays. The excitation function with variable power levels among transducers in arrays is also introduced. The predictive results using the analytical model for the distribution of circumferential displacement amplitudes over time are verified using the finite element method and a CLV-3D laser vibrometry measurement on a 219.1-mm-outer-diameter steel pipe without defect. A comparison between calculated and test results has been analysed

quantitatively. The respective results are in good agreement. Thus, predictions for the superposed wavefield can be used to analyse the realistic characterisation of the excitation function in axial multiple transducer arrays. Additionally, a sensitivity analysis for part-circumferential crack detection using the quasi-axisymmetric torsional modes generated is also evaluated using finite element modelling.

Keywords

Modal superposition, Finite element analysis, Laser velocimetry, Piezoelectric transducer arrays, Guided waves, pipelines.

1. Introduction

The use of guided waves with its features has been widely used to inspect engineering structures for defects [1]-[4] and structural health monitoring (SHM) [5, 6] in industries. In commercial systems, a relatively low-frequency guided wave with a simple mode shape (axisymmetric) is excited. Currently, the commercial systems have successfully used to offer 100% cross-sectional area screening for loss for the pipe wall material [7, 8]. The operating frequencies between 20 kHz and 100 kHz are typical for the guided wave excitation to achieve long-range ultrasonic testing (i.e. many tens of meters). The sensitivity of most applications is in the region of 3-5% [9] metal loss of the pipe wall cross-section on oil and gas pipelines. However, it is still a challenge for improving its performance due to the complexity of guided wave mode excitation and propagation along with a hollow cylindrical structure. A pipe has fundamental axisymmetric wave modes and their families, non-axisymmetric wave modes at a low frequency. Gazis [10] has investigated that they exist in three types which are longitudinal, torsional and flexural in a tubular structure. In the operating frequency range, these wave modes are possibly generated, and the flexural (non-axisymmetric) wave modes are dispersive because their velocities are variable in the frequency range, causing the transmitted pulse to travel with a coherent noise level. Consequently, the reflection from a feature will involve an

unexpected signal-noise ratio by examining responses.

Silk and Bainton [11] identified a naming convention of $Y(m,n)$ to describe these axisymmetric and non-axisymmetric wave modes, in which Y is a letter to represent wave mode characteristics, namely L, T or F for longitudinal, torsional or flexural, respectively, depending on the type of displacement of the wave mode. The term m is the order of cyclic variation on the pipe circumference, and n is an index of modes that occurs with increasing frequency. As shown in Fig. 1, the axisymmetric wave mode L(0,1) has a dominant longitudinal displacement. The axisymmetric wave mode L(0,2) also has the same dominant displacement, but the mode shape is the second type. Furthermore, the axisymmetric wave mode T(0,1) has a dominant torsional displacement. Each of the three types of axisymmetric wave modes has a group of non-axisymmetric wave modes. They are known as higher-order flexural wave modes that have similar displacement characteristics to respective fundamental axisymmetric wave modes. Many non-axisymmetric wave modes are launched instead of a single axisymmetric wave with its complexity on a cylindrical structure when non-axisymmetric transducer arrays are excited synchronously. A set of transducers is designed to distribute equally on the pipe circumference for suppressing non-axisymmetric wave modes. However, many commercial tools are not achieved perfectly to satisfy a transmitter with a 360-degree uniform loading on the pipe circumference [12]. It also exists an energy imbalance for each transducer of transducer arrays in field measurements. When the transducers are driven synchronously, a non-axisymmetric wave is formed from the transducer array excitation owing to wave superposition with axisymmetric and non-axisymmetric wave modes. However, the imbalanced excitation exists in partial transducers of an inspection system, so the displacement amplitude distribution is approximate axially symmetric on the pipe circumference, which is called a quasi-axisymmetric wave. The issue of excitation via ‘partial circumferential loading’ was first studied by Ditri and Rose [13], and they proposed the normal mode expansion (NME) method,

analysed the wave fields in the cylinder in the form of a sum of an infinite number of normal modes. Later, Rose and his colleagues presented their work [14], [15] on the guided waves generated by both axisymmetric and non-axisymmetric loading theoretically and experimentally. Sanderson and Catton [16] presented an analytical model for guided wave inspection optimisation for prismatic structures of any cross-section. The analytical model to one potential application is the optimisation of part-circumferential arrays, and the model has been successfully validated using FE numerical simulations and experiments. However, the results have not clearly confirmed the effectiveness of the proposed methods on the influence of a pipe inspection system under many unexpected conditions. Therefore, it is highly essential to improve a theoretical approach to investigate the realistic transmitter source condition for guided wave excitation. For example, the power normalisation problem of transducers occurs on the current pipe inspection systems composing of two or three rings of transducers and even more in the axial direction.

In this paper, a realistic superposition model of Lamb wave mode shapes in a cylindrical structure based on a normalised NME method and the linear superposition of multiple Lamb waves, and finite element (FE) analyses in Abaqus are used to investigate the effects on the unidirectional enhancement for torsional $T(0,1)$ wave mode excitation using a commercially available tool incorporating three circumferential arrays, or “rings”. Both predictive and experimental works are focused on the guided waves generated by non-uniform surface loading in the circumferential direction. The empirical studies are carried out using the tool (i.e. collars) with 24 thickness-shear (d15) piezoelectric (PZT-5H) transducers in each ring. The predictive results for the distribution of displacement amplitudes over time are verified using CLV-3D laser vibrometer measurements. The comparison between calculated and test results have been enlarged and analysed quantitatively. The sensitivity analysis for part-circumferential crack detection is evaluated using torsional wave modes generated by imbalanced excitation

functions is also evaluated using FE simulations. Compared with FE simulations, the proposed model as a fast solution method has many specific potential applications, such as some quantitative studies of transducer array arrangement, including wave mode excitations, signal waveforms, frequencies, transducer array numbers and spacings. The proposed method can also predict the effects of uncertainty characterization of excitation and propagation of guided waves. The predictive results are necessary for the optimisation of new transducer arrays.

2. Analytical Method

Based on the NME technique [12, 13], the weighting factor $A_+^{mn}(\omega)$ of non-axisymmetric wave modes in the frequency range can be calculated using a normalised weighting function and is given by:

$$\omega_i = 2\pi f_i \quad (1a)$$

$$\mathbf{k}^{mn}(\omega) = \frac{\omega_i}{c_p^{mn}} \quad (1b)$$

$$A_+^{mn}(\omega) = A_+^{0n} \cdot \frac{\sin(m\alpha)}{m\alpha} \cdot \frac{\sin[(\mathbf{k}^{mn}(\omega) - \mathbf{k}^{0n}(\omega))L]}{(\mathbf{k}^{mn}(\omega) - \mathbf{k}^{0n}(\omega))L}, \quad m=1,2,3,\dots \quad (1c)$$

where ω_i is the angular frequency at the corresponding frequency of f_i , the term of $\mathbf{k}^{mn}(\omega)$ is the vector of the angular wavenumber of wave modes $Y(m,n)$ with the vector of its phase velocity, c_p^{mn} as a function of angular frequency, ω and then assuming the weighting factor of the axisymmetric wave mode, $A_+^{0n} = 1$ ($n = 1$) as the incident wavenumber in the frequency range. The vector of the angular incident wavenumber $\mathbf{k}^{0n}(\omega)$ is corresponding to frequencies at the frequency spectrum of the incident time-domain signal. The surface loading of a single transducer is uniformly distributed in the excitation 2α (circumferential length) \times $2L$ (axial length) region (see Fig. 2).

The received distance-trace at any distance of wave propagation can be evaluated by considering the phase shift of frequency components. Equation (2) has described the

summation of all generated guided wave modes weighted by their corresponding amplitude factors and their dispersive propagation in the z -direction on structure, as given by:

$$V(z) = \sum_{n=1}^{\infty} \sum_{m=0}^{\infty} \int_{-\infty}^{\infty} A_+^{mn}(\omega) \cdot U(\omega) e^{-ik^{mn}(\omega)z} d\omega \quad (2)$$

where $U(\omega)$ is the fast Fourier transform (FFT) of the input pulse in the time domain, $u(t)$. The function of $U(\omega)e^{jk^{mn}(\omega)z}$ is dispersive propagation on the hollow structure in distance-trace. The angular profile illustrates the total displacement distribution resulting from a linear superposition of an array of multiple transducers around a pipe circumference. The function of particle displacement amplitudes at any position of cylindrical structures in the circumferential direction is given by [16, 17]:

$$A_d = \cos(m(\theta_i + \theta)) \quad (3)$$

where A_d is the angular distribution function of the particle displacement created by generated wave modes in the circumferential direction. The term θ_i is the circumferential position of element i for excitation and θ is the target position (monitoring point) of the field. For $m = 0$, the mode is axisymmetric torsional. For $m > 0$, the mode is torsional-type flexural.

Combining (2) and (3), the total angular profile $\mathbf{h}(\theta_i + \theta, t)$ at distance $z = z_0$ (z_0 represents any propagation distance in the axial direction) is the linear superposition of all of the elements' angular profiles (up to N_T) at that distance in the time domain. The function of dispersive wave propagation can be given using superposition of the received distance-trace $U(\omega)$, converting to time-trace depending on its inverse fast Fourier transform (IFFT):

$$\mathbf{h}(\theta_i + \theta, t) = \sum_{i=1}^{N_T} a_i \cdot \int_{-\infty}^{\infty} \left[\sum_{n=1}^{\infty} \sum_{m=0}^{\infty} A_+^{mn}(\omega) \cdot U(\omega) e^{-ik^{mn}(\omega)z_0} \cdot \cos(m(\theta_i + \theta)) \right] e^{j\omega t} d\omega \quad (4)$$

where $\mathbf{h}(\theta_i + \theta, t)$ represents the function of circumferential displacement amplitudes at any position of the field at the outer surface of the circumference after any propagation distance, z_0 away from multiple loadings on the pipe circumference in the time domain, N_T is the number

of transducer elements in an array and a_i is the amplitude factor for the power output of one transducer element. The total angular profile of an array with multiple rings, N_r of transducers with the shifted input signal can be expressed as (see Fig. 3):

$$A_{\max}(\theta) = \max \left| A_i \cdot \sum_{i=1}^{N_r} h(\theta_i + \theta, t - t_i) \right| \quad (5)$$

$$t \in [z_0 / c_T, z_0 / c_T + n_c / f_c].$$

where A_i is the amplitude factor of the input signal pulse for one ring, and $t_i = N_i(R_s/c_T)$, where R_s is ring spacing, c_T is the torsional velocity and N_i is the i -th number of rings in axial multiple transducer arrays.

3. Finite Element Modelling for Circular Point Sources on a Pipe

To predict a realistic excitation function of the commercial pipe inspection system [17], numerical modelling is used to investigate the performance of guided wave testing by using the transducer arrays with a 33-degree gap. The numerical simulation for the guided wave method on a 7 m long, 219.1 mm outer diameter, 8.18 mm wall thickness steel pipe for defect detection is conducted using a commercial finite element analysis software, Abaqus (6.14-4). In the FE models, the Explicit module is used to produce a transient wave field. The material property of steel pipe is modelled as a linear isotropic material with a mass density $\rho = 7932$ kg/m³, Young's modulus $E = 216.9$ GPa and Poisson's ratio $\nu = 0.2865$. Three rings of transducers in a sequence are installed along the pipe, and the front ring (Ring1) is placed 1.8 m away from the left pipe end. As with the tool, the ring spacing is 30 mm, and each ring has 24 transducers uniformly spaced on the circumference except for a 33-degree gap between transducers No.1 and No.24. Twenty-four transducers in each ring are separated into eight segments, and then every three transducers become a group, as shown in Fig. 4.

3.1 Hanning Windowed Signal Pulses

In order to inspect reflections from features on structures for ultrasonic guided wave testing, the excitation of the incident signal is often a pulse with several cycles. With an increased number of cycles, it can reduce the frequency bandwidth of the pulse so that the incident wave is less dispersive for propagating over a distance. The unidirectional excitation can be achieved by phasing the transmitted signals received from multiple rings [18]. In general, wave modes can be created using a loading source in any direction. Then a unidirectional excitation and propagation of guided waves can be obtained, depending on amplitude factors, time delays and excitation positions. The function $u_i(t)$ can determine an input signal pulse for each ring of transducers, given by

$$u_i(t) = A_i \cdot \frac{1}{2} \left[1 - \cos \frac{2\pi f_c (t - (N_i - 1) \cdot (R_s / 2c_T))}{n_c} \right] \cdot \sin \left(2\pi f_c (t - (N_i - 1) \cdot (R_s / 2c_T)) \right) \quad (6)$$

where t is the time, f_c is the centre frequency of the incident signal, and n_c is the number of cycles for the Hanning windowed signal. Generally, narrowband signals are used in a 5-cycle or 10-cycle Hanning window [19]. Therefore, a 10-cycle, 35 kHz Hanning windowed signal as the incident pulse can be selected to excite torsional wave modes. In the three-ring system with a 30 mm ring spacing, the input waveforms are calculated using (6) for each ring, and the normalised displacement amplitudes in the time domain shows in Fig. 5(a). The amplitude factor of the input signal pulse, $A_1 = 1$ is given for the front ring. The excitation is inverted ($A_2 = -1$) with a delayed time (4.6 us) for the middle ring excitation. Then the unconverted signal ($A_3 = 1$) has a delayed time (9.2 us) that is excited by the back ring. The waveforms for the input signals are used in numerical FE simulations and experiments.

3.2 Dispersion Curves

Generally, the superimposed packet as a Hanning-windowed pulse travels with the group velocity c_g , whereas the phase velocity c_p is the speed at which a single frequency component

of the pulse. For example, the individual harmonic waves travel with different phase velocities through the structure. In this paper, the phase and group dispersion curves are calculated numerically by a semi-analytical finite element (SAFE) method [20], as shown in Fig. 6. Characteristic velocities are compressional (longitudinal) bulk wave velocity $c_L = 5960$ m/s and shear (torsional) bulk wave velocity $c_T = 3260$ m/s of the waveguide. Generally, the selected wave modes for guided wave testing in pipe inspection are torsional wave mode T(0,1), longitudinal wave modes L(0,1) and L(0,2). The torsional wave mode T(0,1) is completely non-dispersive with a constant velocity in a range of frequencies. These three wave modes are followed by their flexural mode families F(m,2), F(m,1) and F(m,3), respectively. Due to its feature, the torsional wave mode T(0,1) is widely used [21]. Therefore, this paper discusses the excitation and propagation of torsional wave modes using the transducer arrays.

3.3 Finite Element Modelling for Circumferential Crack Detection

To investigate the influence of the imbalanced transducer excitation in arrays for pipe inspection, the numerical finite element modelling combined with the predicted wavefield of guided wave based on the developed analytical model for simulating circumferential crack detection. The hybrid method, as a fast technique, can evaluate the sensitivity analysis for part-circumferential crack detection using the generated quasi-axisymmetric torsional modes. In numerical FE simulations, the transducers are all simulated as point sources. The loading in the tangential direction at each point is to excite the first torsional wave mode T(0,1). The input pulse is a 10-cycle 35 kHz Hanning-windowed pulse and the frequency bandwidth of ± 7 kHz. The incident waves from each ring with time-delayed and shifted superpose each other to lead the signal propagation directionality. The method is called the unidirectional excitation of guided waves [18], [21]. Therefore, the waveforms in Fig. 5(a) for each ring are generated and propagated for cancelling the backward signal. The receivers, composed of 24 equally spaced points, are placed 1.7 m away from the Ring1 for measuring displacement amplitudes in

cylindrical coordinates. The transducer No.1 at each ring and receiver No.1 are all arranged at 90-degree in the cross-section area (CSA) of the pipe.

To further evaluate guided wave excitation by using transducer arrays with the energy imbalance problem, segment C of the transducer arrays (see Fig. 4) is assumed to be no transmission to compare the predictive results with the results using the transducer arrays. Consequently, the transducer arrays with a 33-degree gap and no transmission at segment C as a transmitter is simulated to excite guided waves for defect detection. Therefore, a part-circumferential crack, 500 μm width in the axial direction and 8.18 mm depth in the radial direction, is simulated with circumferential growth. The part-circumferential cracks are located 1.7 m away from the array of 24 receivers. In FE models, the mesh size is defined to satisfy at least eight elements per wavelength for accurate results. Therefore, to ensure the finite element models have satisfactory accuracy, the element size is defined as 4 mm in the axial direction, and the element number is refined to four in the radial direction to capture displacement variations for higher-order wave modes. Furthermore, Table 1 indicates the set-up of the total element quantity and the mesh element of a part-circumferential crack for each case.

The pulse is excited, and torsional type waves propagate along with the pipe model. Time increment size is around 53 ns. The duration of the transmitted pulse is 295 μs , and the total calculation time is around 5.3 ms. Therefore, it is up to 1,217,140 hexahedron elements (element type C3D8R) to be generated, taking around 12 hours to complete the full analysis for each excitation.

The case study is undertaken to simulate guided wave testing for a through-thickness crack with a 4.17% CSA on the pipe. Figure 7 shows the predictive results at receiver No.1 for variation of normalised displacement amplitudes in circumferential, radial and axial directions over time. The recorded time is 3.35 ms. The results show that the resultant wave is excited unidirectionally in the circumferential direction by using three rings of transducers with a 30

mm ring spacing, depending on incident waveforms in each ring. Regarding the predictive results of the comparison between transducer arrays with a 33-degree gap (black) and transducer arrays with a 33-degree gap and no transmission at segment C (red), as shown in Fig. 7, it can be found that the amplitude of torsional wave mode $T(0,1)$ reduces in the circumferential direction. Higher-order flexural wave modes $F(m,2)$ are generated and superimposed with the transmitted wave mode $T(0,1)$. Meanwhile, the flexural waves show dispersive behaviour because these differences in speed cause the spreading of wave packets along the pipe length over time. Later, the transmitted waves scatter after reflection from the partial circumferential crack, and the flexural wave modes $F(m,3)$ appear to superpose the reflected wave. Afterwards, the amplitude of the $F(m,2)$ and $F(m,3)$ modes distinctly increase in the circumferential and axial directions (see Fig. 7(a) and 7(c)) after reflection through the end face of the pipe due to no signal transmission at partial transducers in the array when compared to the transducer arrays with a 33-degree gap.

Figure 8 shows the predictive results by summing and normalizing signals recorded at 24 receivers around the pipe circumference in the time domain. It shows an increased reflection coefficient trend in the circumferential direction as the part-circumferential crack size increases with the two different excitation functions for the wave mode $T(0,1)$ at the central frequency of 35 kHz. The reflection coefficients reduce when the transmitter with no signal transmission at segment C. Meanwhile, the difference between two different excitation functions is increased slightly as the crack circumferential size grows. As a result, the energy of the fundamental wave mode reduces, and its higher-order wave modes increase after the signal reflection from a part-circumferential crack when the imbalanced excitation of guided waves in circumferential transducer arrays.

Figure 9 illustrates angular profiles of the torsional wave mode $T(0,1)$ superimposed with higher-order flexural modes for the transmitted and reflected signals from two different

excitation functions (shown in Fig. 9(a)) and three different circumferential crack sizes (shown in Figs. 9(b)-(d)). Figure 9(a) shows an angular profile for predictive results of normalised circumferential displacement amplitudes of torsional type wave modes. The results are recorded at 1.7 m away from the Ring1 to describe the particle displacement distribution of the exciting wave modes, depending on 24 independent monitoring positions on the pipe circumference. The results show that the quasi-axisymmetric waves are generated owing to the imbalanced excitation function. Furthermore, it also can be seen that the particle displacement amplitude reduces significantly at the positions with no signal transmission. Figures 9(b)-(d) show that the related data are located 1.7 m away from the cracks. The angular profile presents the energy distribution of the reflected wave that can determine the crack characteristics, such as size and location. Figure 9(b) shows that the crack size is smaller than the gap size and the circumferential crack area is within the no signal transmission range. Therefore, the gap range influences the effect of the reflection from the defect in angular profiles. Meanwhile, the amplitude of flexural wave modes $F(m,2)$ increases at between 180 degrees and 210 degrees for no transmission at segment C, but the total energy is still lower than the excitation function with a 33-degree gap only due to the reduced excitation points. However, as shown in Figs. 9(c)-(d), the angular profile changes clearly as the crack changes. Although the total energy of the reflected wave reduces, a similar trend for the amplitude distribution can be generated with the excitation function without signal transmission at segment C because the number of monitoring points can be used to determine the circumferential orders of all generated guided wave modes.

4 Validations

The 3D analytical model for simulating the imbalanced excitation of guided waves with circular transducers is verified using a test rig set up for the generation and measurement of guided wave modes. Firstly, the FE modelling for the investigation of guided wave excitation

and propagation for pipe inspection is to compare the analytical predictions. Then both results are examined using the experimental data with the variable amplitude factor for the power of transducers at segment C in the collar (see Fig. 10(b)). In FE models, there are 1,211,692 hexahedron elements (element type C3D8R) to be generated, taking around 12 hours to complete the full analysis for each excitation. The amplitude factor for the power of three transducers at segment C in the collar is reduced from 1.0 to 0 with a step decrement of 0.2. Experiments (illustrated in Fig. 10(a)) using a robotic CLV-3D laser vibrometer were carried out for the pipe shown in Fig. 11. Due to the torsional wave modes were excited by thickness-shear (d15) piezoelectric (PZT-5H) transducers, an inflatable collar was designed to apply pressure to the pipe surface for assuring firm contact in this experiment. The input pressure of 60 psi provided by using an air pressure control system to the collar loaded the transducers onto the surface of the pipe in the experiment. The collar with 24 transducers in each ring was clamped on a 7 m long, 219.1 mm outer diameter, 8.18 mm wall thickness steel pipe so that a non-axisymmetric loading was generated on the pipe circumference because the collar had a gap of 33-degree between the first and last transducer. However, the rest of the 22 transducers were equally spaced at each ring. The tool composed of three rings of transducers with a 30 mm ring spacing, was driven by a Teletest®Mk3 system. The excitation region 13 mm × 3 mm was used, and the loading in the circumferential direction was to generate torsional wave modes. The transmitted signal was measured using a CLV-3D laser vibrometer. The CLV-3D optical sensor head contains the optical components of three independent laser Doppler vibrometers. The monitoring position of the optical sensor head was controlled through the pathway by the robotic system. The location of the sensor head was fixed vertically at 3.4 m away from the Ring1 of the tool. The laser vibrometer measured circumferential displacements at 24 reflective patches equally distributed around the pipe circumference because the displacement amplitudes

of torsional waves are dominant in the circumferential direction when the wave modes propagate along a pipe.

The time-domain waveforms predicted by the proposed model, the FE model and collected data from experimental measurements at 24 equally spaced monitoring positions are provided and compared, as shown in Fig. 12. There is a good agreement between each other's results about the received signal time being revived and the circumferential displacement amplitudes of the wavefield obtained at a 3.4 m distance. It also can be found that the wave field has a significant amplitude level for some higher-order wave modes $F(m,2)$ (typically $F(1,2)$ to $F(3,2)$) following the zero-order wave mode $T(0,1)$. As a result, the transmitted signal increased a coherent noise level to influence the inspection system resolution. Under this circumstance, the device will be difficult to find a lower reflective amplitude level from a minor defect. However, the wave mode number can be known at a given frequency based on its dispersion curves. Then, the theoretical model calculates the factor amplitude of undesired wave modes. Then, the wave field of the quasi-axisymmetric waves depending on the different transducer arrangements and power outputs in arrays that can be predicted with a low computational load. In addition to the influence of the transducer arrangement in arrays, the unidirectional guided wave excitation effect for defect detection is also influenced by the ring spacing between each ring and the excitation frequency. An analytical and experimental investigation of the influence of ring number and distances in an array of transducers was presented in [21]. This paper focuses on the effect of quasi-axisymmetric torsional waves generated from the arrays of transducers at a fixed ring spacing.

Figure 13 shows the comparison of the normalised circumferential displacements in angular profiles obtained at 3.4 m away from the Ring1 of the collar from experimental measurements, analytical and numerical simulations. The developed analytical model based on the NME method is employed. Results show that the commercial tool was driven but did not achieve

perfectly to satisfy a transmitter with an axisymmetric loading. The quasi-axisymmetric waves were generated because of the non-axisymmetric transducer spacing in transducer arrays. The energy distribution of the transmitted wavefield significantly changes when the value of the amplitude factor for segment C reduces. Therefore, it is highly essential to consider guided wave excitation with an energy imbalance problem among transducers in arrays. Table 2 indicates a less than 20% error for analytical to FE simulations and a less than 15% error for both analytical and FE numerical simulations to experiments. From the results, the predicted values from the analytical and FE numerical models have good agreement with the measured data given by using laser vibrometer measurements.

5. Conclusions

This paper aims to develop a fast analytical model for an investigation into the wave field prediction of the guided Lamb wave mode superposition influenced on a realistic pipe inspection system of axial multiple transducer arrays under many unexpected conditions. The finite element method is already used to simulate a transducer or transducer arrays for guided wave excitation, but it can take many hours to compute a solution. The modelling method uses the normalised NME method to extract the amplitude factors of Lamb wave modes generated on a single transducer element and then use the information in a linear superposition method to provide a three-dimensional wavefield with a cylindrical structure at axial positions. The model successfully simulates the unidirectional excitation function for the generation of torsional guided waves using the transducer array with multiple axial rings. The non-uniform excitation and imbalanced energy transmission problems in an array of transducers are predicted successfully using the proposed approach. The analytical results are compared to FE numerical predictions and then validated experimentally. The predicted values from the analytical and FE numerical models have good agreement with the measured data. Therefore, the method could be useful for the investigation into the effects of excitation and propagation

of guided waves under different conditions that are not currently fully understood, such as the linear superposition problem of variable power levels from each transducer in arrays. Uncertainty characterization of transducer arrays could also be quantified quickly to predict the influence of the generation of ultrasonic guided waves successfully. Thus, it impacts the pipe inspection performance of guided waves and the development of advanced transducer arrays. Additionally, three different circumferential cracks are simulated to investigate the influence of part circumferential loading on a pipe for defect detection in FE simulations. The reflection coefficients of increased part-circumferential crack sizes are analysed with different imbalanced excitation functions. The appearance of high flexural order modes is clear. The $T(0,1)$ with them show high sensitivity to the circumferential defect. The angular profile of torsional type wave modes represents a non-axisymmetric energy distribution on the pipe circumference.

Acknowledgments

This publication was made possible by the sponsorship and support of TWI Ltd. and the University of Greenwich. The work was enabled through, and undertaken at, the National Structural Integrity Research Centre (NSIRC), a postgraduate engineering facility for industry-led research into structural integrity established and managed by TWI through a network of both national and international Universities.

REFERENCES

- [1] D. N. Alleyne, M. J. S. Lowe, and P. Cawley, "The reflection of guided waves from circumferential notches in pipes," *J. Appl. Mech.*, vol. 65, no. 3, pp. 635-641, Sep. 1998.
- [2] D. N. Alleyne, T. Vogt, and P. Cawley, "The choice of torsional or longitudinal excitation in guided wave pipe inspection," *Insight-Non-Destructive Testing and Condition Monitoring*, vol. 51, no. 7, pp. 373-377, Jul. 2009.

- [3] A. Klepka, W. J. Staszewski, T. Uhl, D. Maio, F. Scarpa, and K. F. Tee, "Impact damage detection in composite chiral sandwich panels," *Key Eng. Mater.*, vol.518, pp.160-167, Jul 2012.
- [4] F. Sagasta, K. F. Tee, and R. Piotrkowski, "Lamb modes detection using cumulated Shannon entropy with improved estimation of arrival time," *J. Nondestruct. Eval.*, vol. 38, no. 1, Feb. 2019.
- [5] P. Cawley, "Practical guided wave inspection and applications to structural health monitoring," in *Proc. of the 5th Australasian Congress on Applied Mechanics*, Brisbane, Australia, 2007, p. 12.
- [6] A. Klepka, W. J. Staszewski, D. Maio, F. Scarpa, K. F. Tee, and T. Uhl, "Sensor location analysis in nonlinear acoustics used for damage detection in composite chiral sandwich panels," *Adv. Sci. Tech.*, vol.83, pp. 223-231, Sep. 2012.
- [7] P. J. Mudge, "Field application of the Teletest long-range ultrasonic testing technique," *Insight*, vol. 43, no. 2, pp. 74-77, 2001
- [8] D. N. Alleyne, B. Pavlakovic, M. J. S. Lowe, and P. Cawley, "Rapid, long range inspection of chemical plant pipework using guided waves," in *AIP conference proceedings*, vol. 557, no. 1, pp. 180-187, Jun. 2001.
- [9] P. J. Mudge and J. Speck, "Long-range ultrasonic testing (LRUT) of pipelines and piping," *Insp. J.*, vol. 10, pp. 1-4, Sep. 2004.
- [10] D. C. Gazis, "Three-dimensional investigation of the propagation of waves in hollow circular cylinder. I. Analytical foundation," *J. Acoust. Soc. Am.*, vol. 31, no. 5, pp. 568-573, 1959.
- [11] M. G. Silk and K. F. Bainton, "The propagation in metal tubing of ultrasonic wave modes equivalent to lamb waves," *Ultrasonics*, vol. 17, no. 1, pp. 11-19, Jan. 1979.

- [12] J. L. Rose, "Guided waves in hollow cylinders," in *Ultrasonic guided waves in solid media*, 1st ed. Cambridge, Cambridge University Press, 2014, pp. 155-173.
- [13] J. J. Ditri and J. L. Rose, "Excitation of guided elastic wave modes in hollow cylinders by applied surface tractions," *Int. J. Appl. Phys.*, vol. 72, no. 7, pp. 2589-2597, May 1992.
- [14] H. J. Shin and J. L. Rose, "Guided waves by axisymmetric and non-axisymmetric surface loading on hollow cylinders," *Ultrasonics*, vol. 37, no. 5, pp. 355-363, Jun. 1999.
- [15] J. Li and J. L. Rose, "Excitation and propagation of non-axisymmetric guided waves in a hollow cylinder," *J. Acoust. Soc. Am.*, vol. 109, no. 2, pp. 457-464. Feb. 2001.
- [16] R. M. Sanderson and P. P. Catton, "An analytical model for guided wave inspection optimization for prismatic structures of any cross section," *IEEE Trans. Ultrason. Ferroelectr. Freq. Control*, vol. 58, no. 5, pp. 1016-1026, May 2011.
- [17] J. Li and J. L. Rose, "Angular-profile tuning of guided waves in hollow cylinders using a circumferential phased array," *IEEE Trans. Ultrason. Ferroelectr. Freq. Control*, vol. 49, no. 12, pp. 1720-1729, Dec 2002.
- [18] X. Niu, W. Duan and H.-P. Chen and H. R. Marques, "Excitation and propagation of torsional T (0,1) mode for guided wave testing of pipeline integrity," *Measurement*, vol. 131, pp. 341-348, Jan. 2019.
- [19] A. Ghavamian, F. Mustapha, and B.T. Baharudin, and N. Yidris, "Detection, localisation and assessment of defects in pipes using guided wave techniques: a review," *Sensors*, vol. 18, no. 12, p. 4470, Dec. 2018
- [20] W. Duan and R. Kirby, "A numerical model for the scattering of elastic waves from a non-axisymmetric defect in a pipe," *Finite Elem. Anal. Des.*, vol. 100, pp. 28-40, Aug. 2015.
- [21] X. Niu, K. F. Tee and H. R. Marques, "Enhancement of unidirectional excitation of guided torsional T(0,1) mode by linear superposition of multiple rings of transducers," *Applied Acoustics*, vol. 168, p. 107411, Nov. 2020.

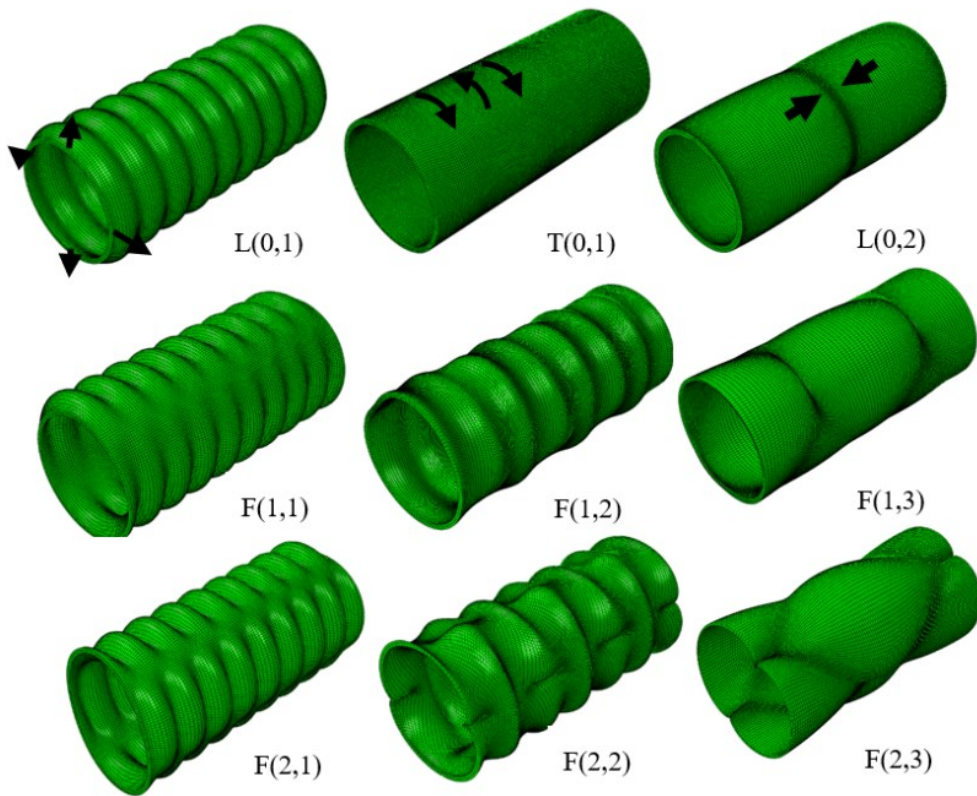


Fig. 1. Cylindrical mode shapes in a 219.1 mm outer diameter, 8.18 mm wall thickness steel pipe at around 20 kHz.

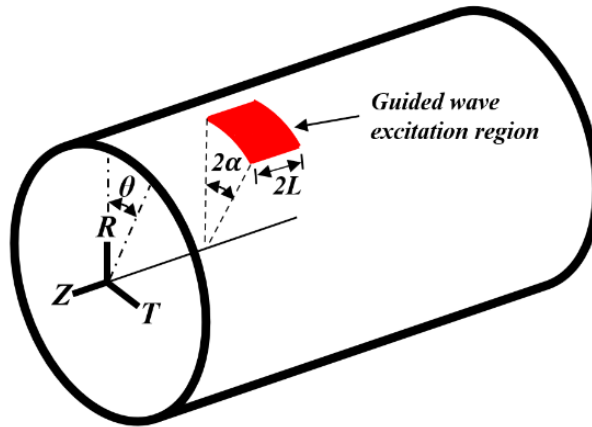


Fig. 2 A surface loading on an elastic isotropic hollow cylinder.

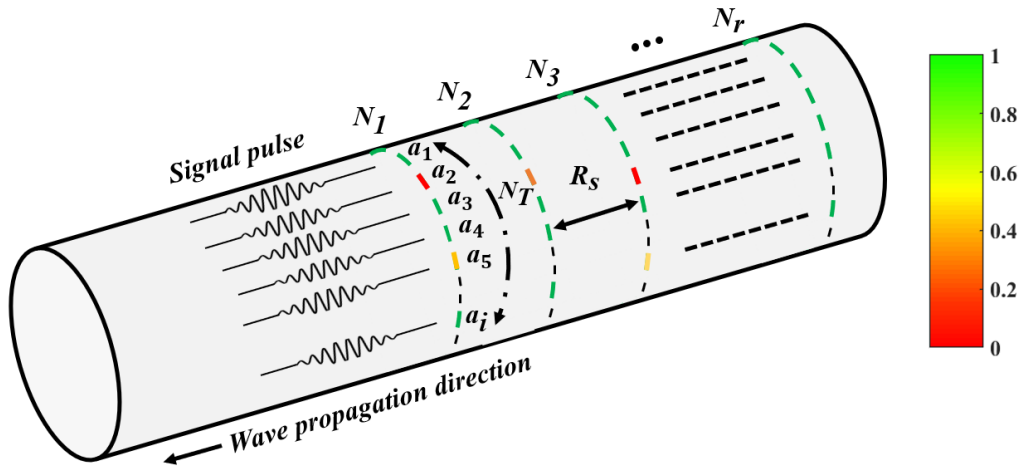


Fig. 3. A schematic design for a three-dimensional analytical model of the imbalanced excitation of guided waves with circular transducer arrays.

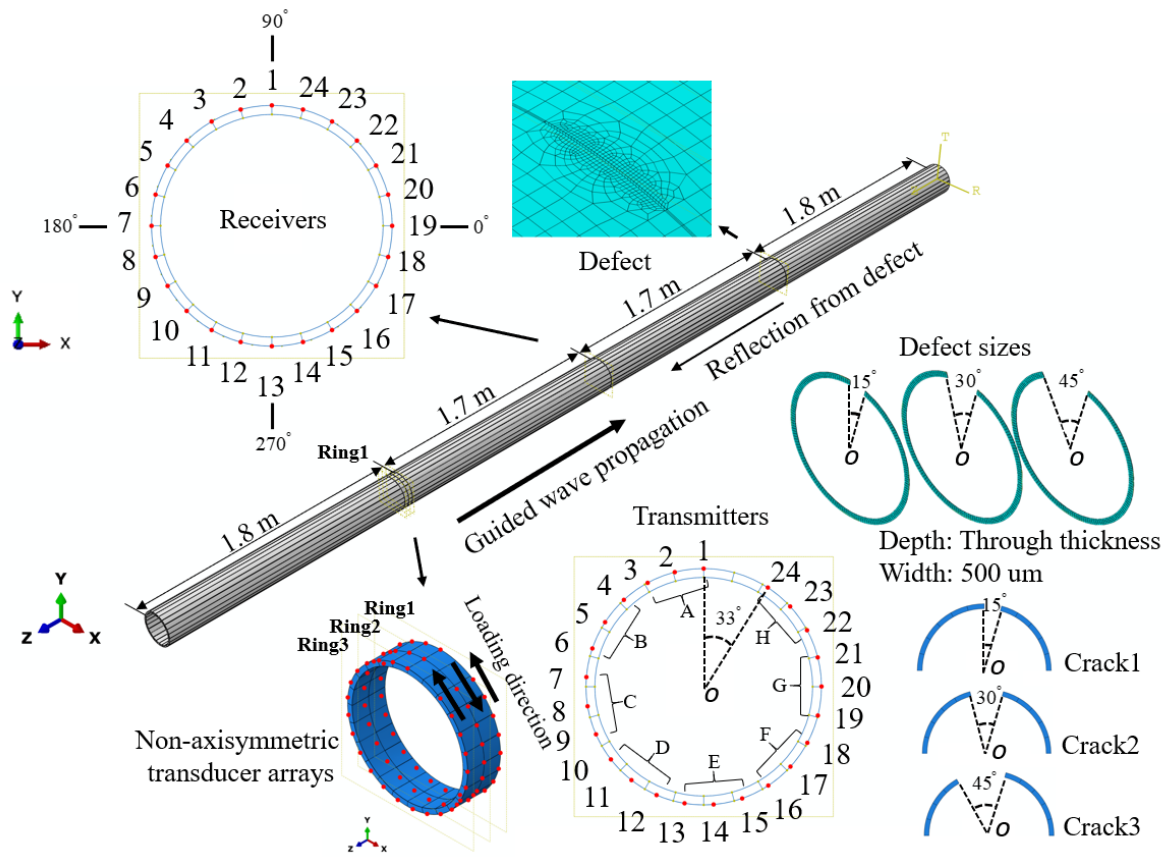


Fig. 4. Finite element modelling for a steel pipe with three rings of transducers for defect detection.

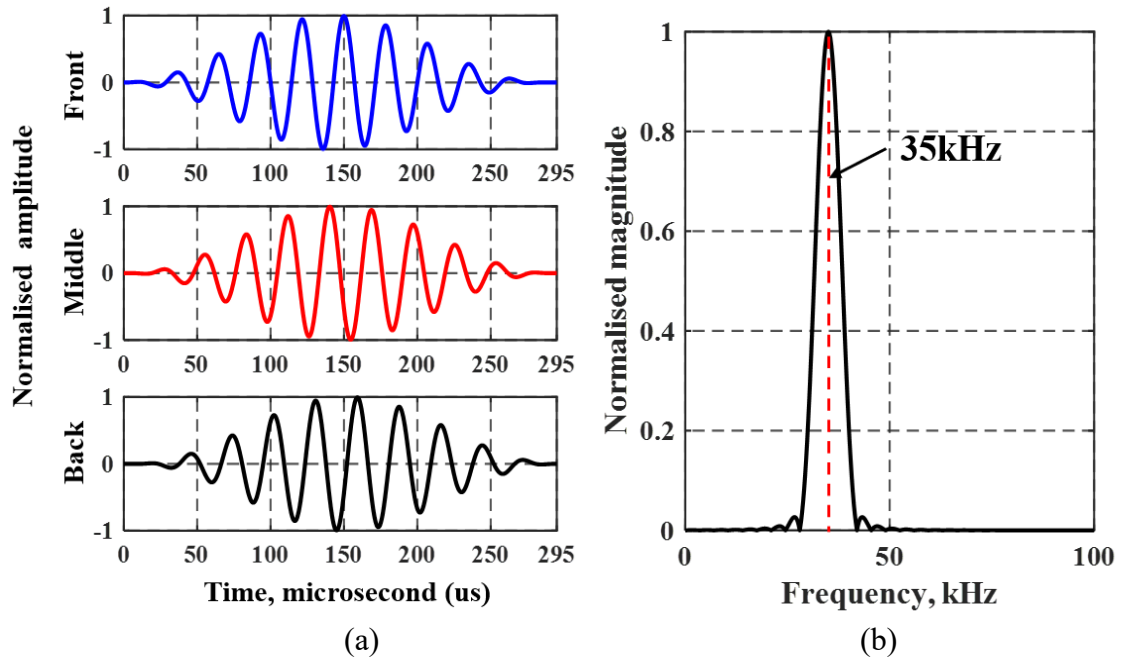
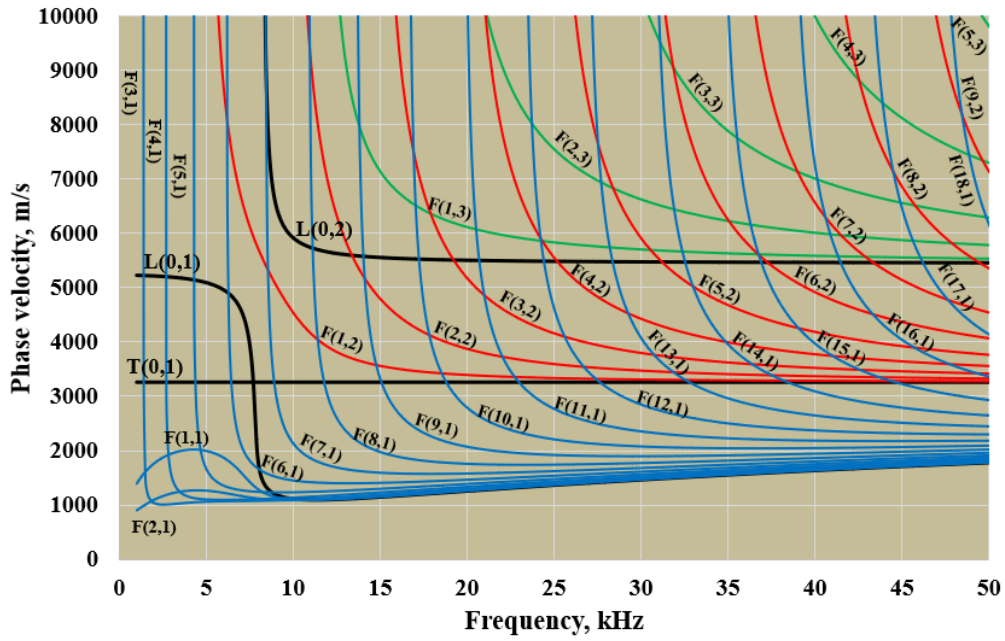
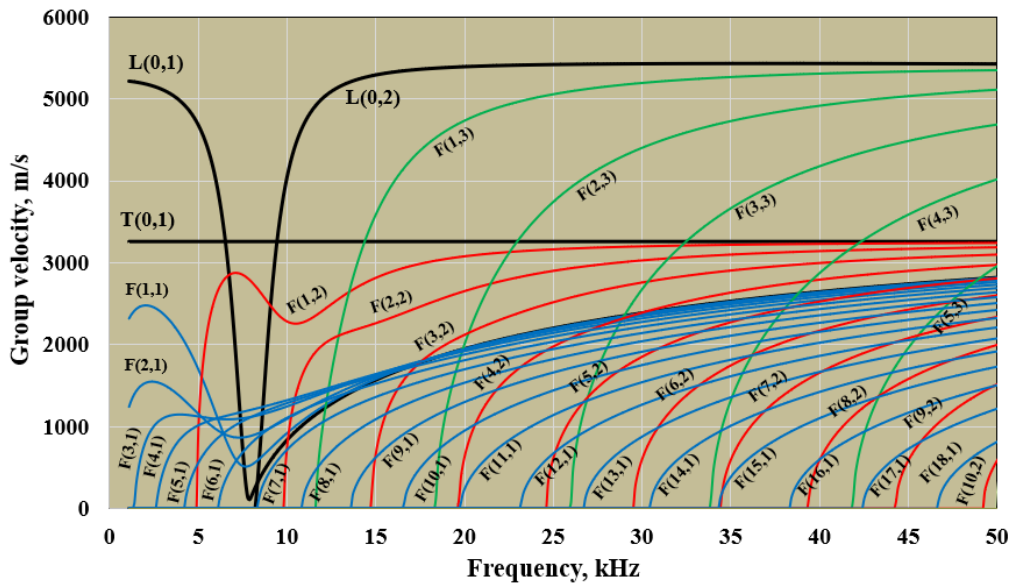


Fig. 5. The incident signal pulses for three rings of transducers, a 10-cycle 35 kHz Hanning windowed signal: (a) time domain, front waveform (blue), middle waveform (red), back waveform (black), (b) frequency spectrum.



(a)



(b)

Fig. 6. Dispersion curves for a steel pipe (219.1 mm outer diameter, 8.18 mm wall thickness): (a) phase velocity, (b) group velocity.

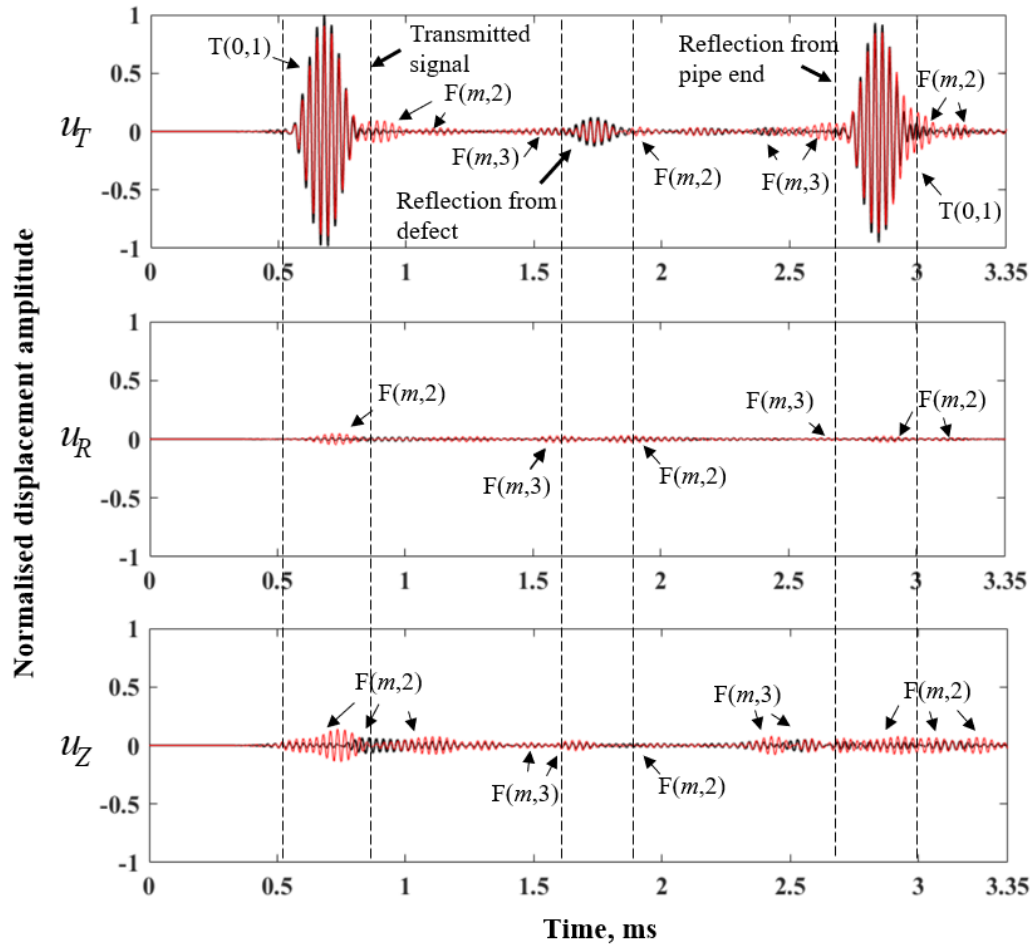


Fig. 7. Predictive results at receiver No.1 for normalised circumferential, radial and axial displacements obtained from numerical simulations for defect detection by using the transducer arrays with a 33-degree gap (black), and transducer arrays with a 33-degree gap and no transmission at segment C (red).

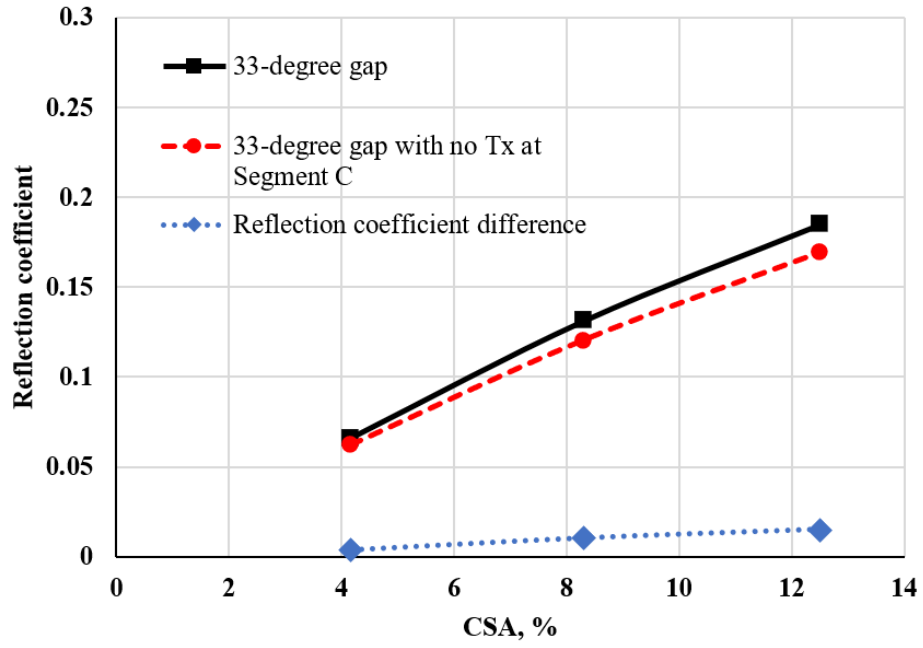


Fig. 8. 3D FE predictions of the reflection coefficient of the guided wave method at circumferential crack lengths in the pipe by exciting wave mode T(0,1) at the central frequency of 35 kHz.

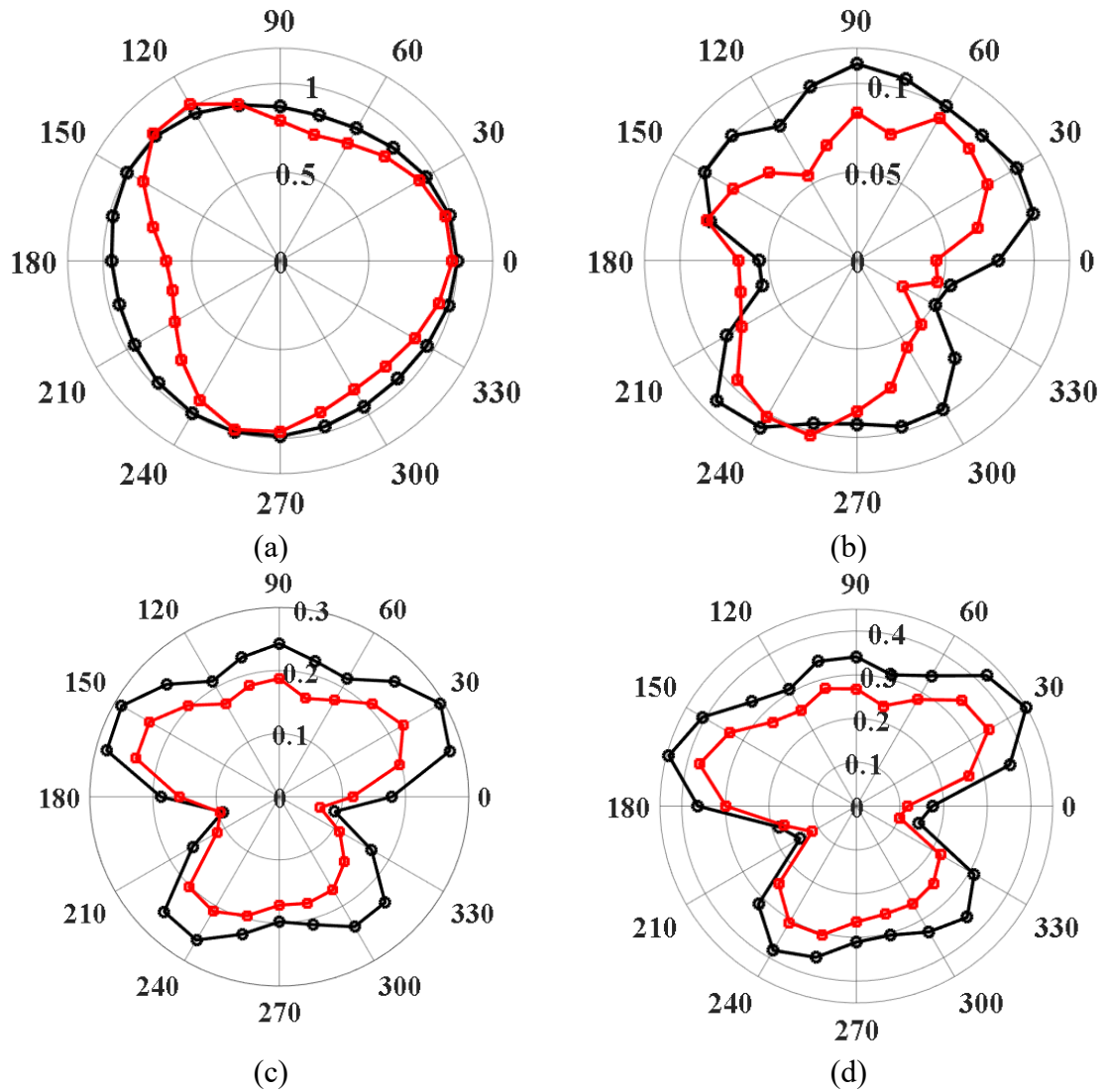
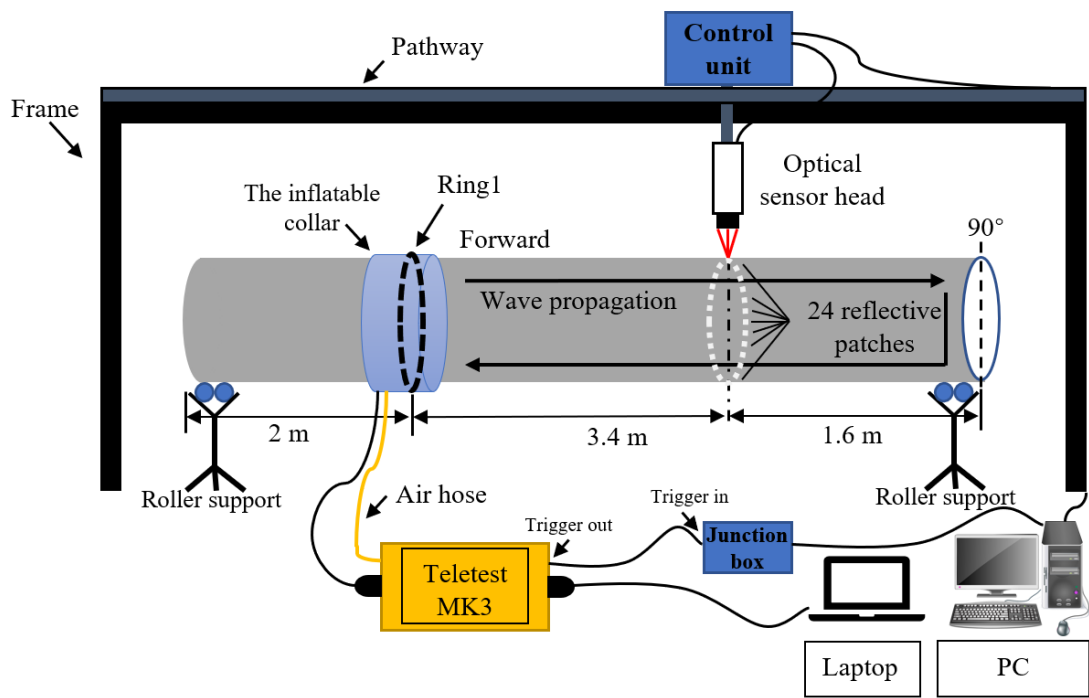
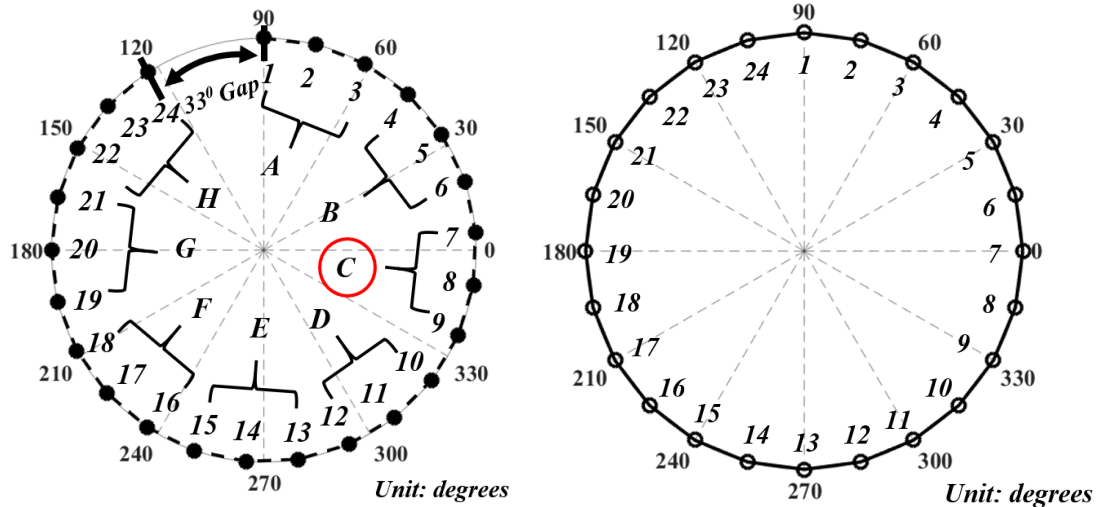


Fig. 9. Angular profile results of guided wave modes in a steel pipe with different crack sizes at $z = 3.4$ m from Ring1 at the central frequency of 35 kHz excited by using, \ominus , three rings of transducers with a 33-degree gap, and \boxminus , a 33-degree gap with no transmission at segment C: (a) $z = 1.7$ m from Ring1, (b) 4.17% CSA, (c) 8.33% CSA, and (d) 12.50% CSA.

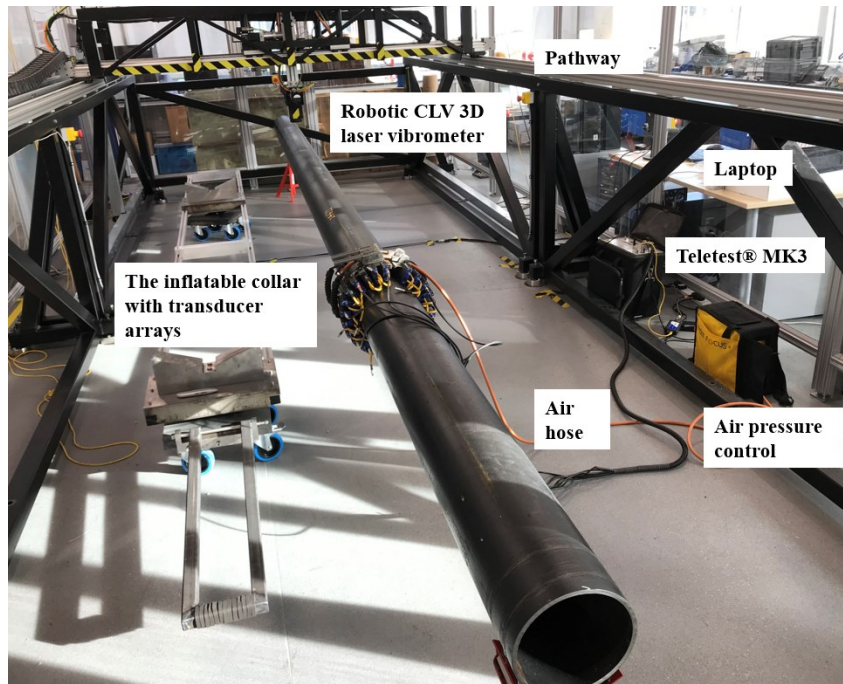


(a)

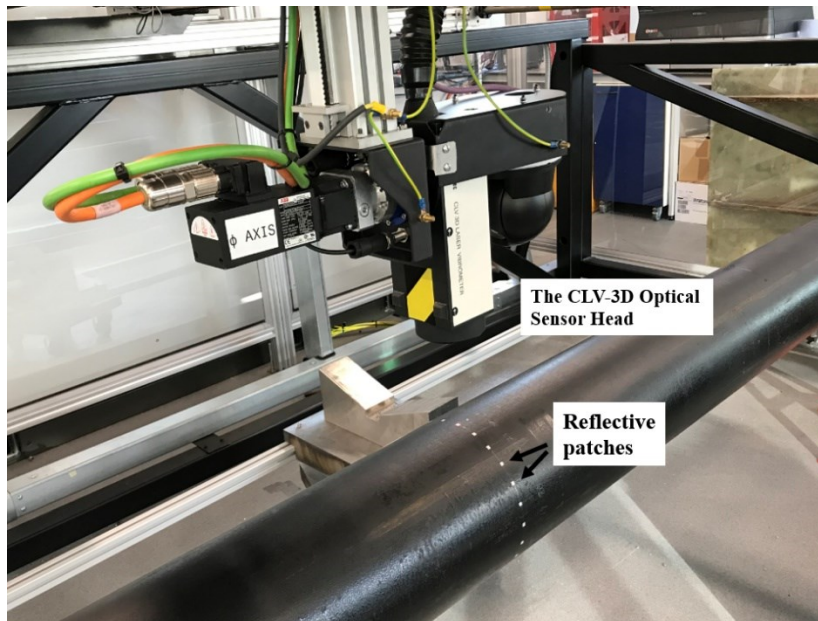


(b)

Fig. 10. A design of robotic 3D-CLV laser vibrometer experiment: (a) schematic diagram of experimental set-up for robotic 3D-CLV laser vibrometer experiment, (b) excitation positions (left) and monitoring positions (right).



(a)



(b)

Fig. 11. Set up of a test rig for generation and measurement of wave modes: (a) full-view (b) robotic 3D laser vibrometer

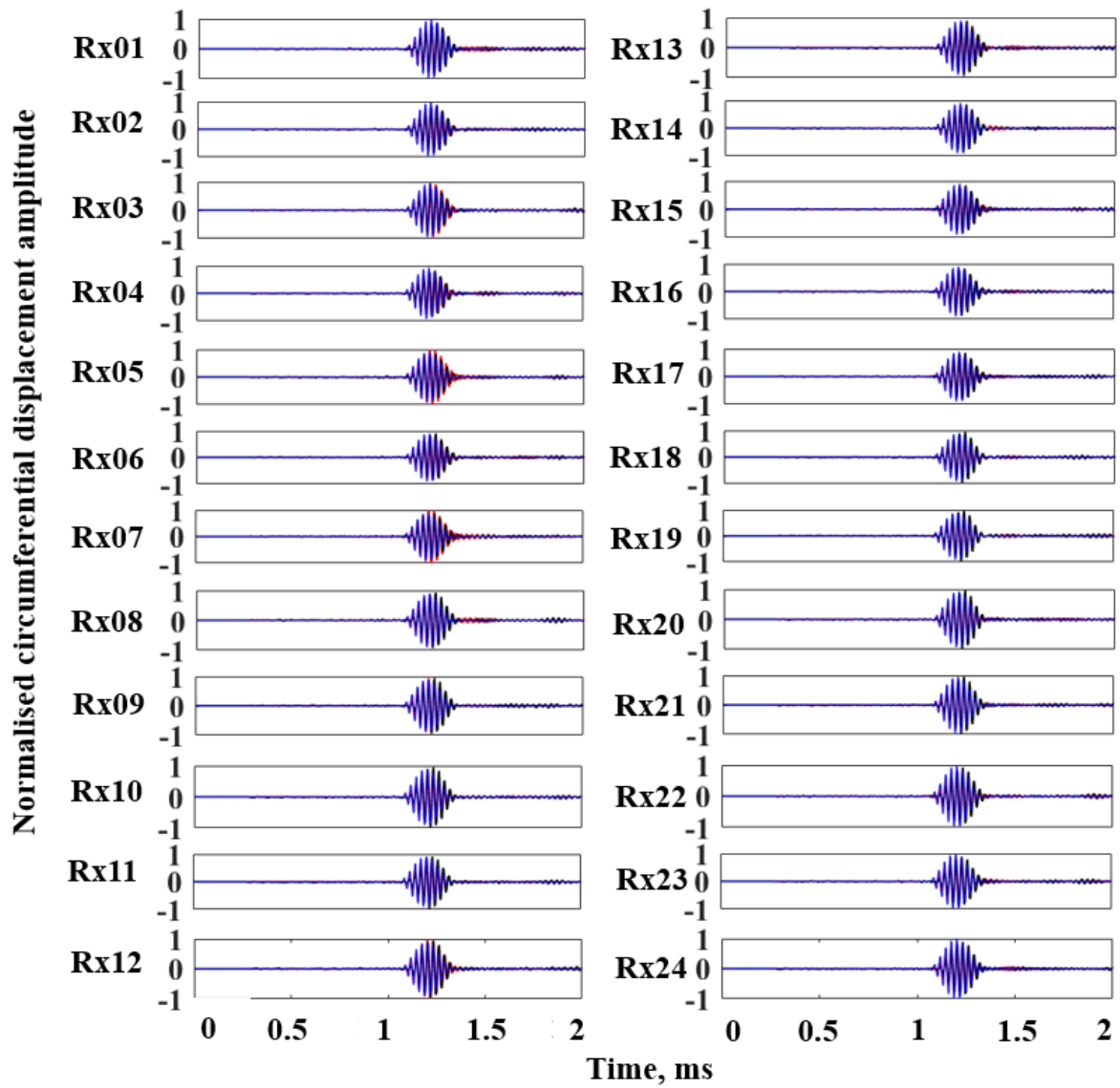


Fig. 12. Normalised circumferential displacements for the wave field in time domain monitored at 3.4 m away from the front transducer ring as the transducer array with a 33-degree gap and the amplitude factor at Segment C is 1.0, —, analytical simulation, —, FE model, —, experiment.

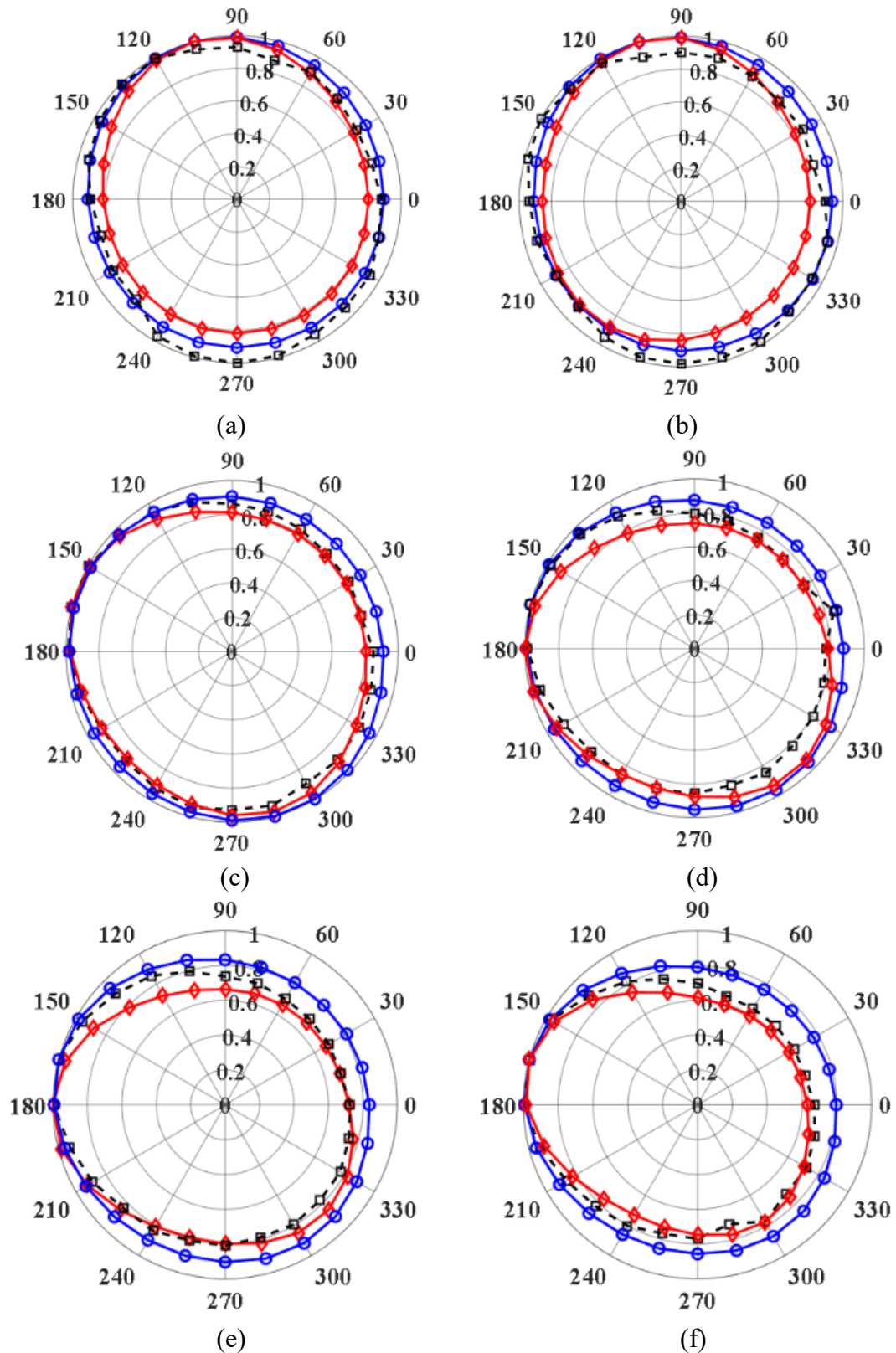


Fig. 13. Angular profile results of normalised circumferential displacements for the energy distribution of wave modes generated along the pipe with the amplitude factor for the power output of transducers at segment C in the collar is reduced from 1.0 to 0 with a step decrement of 0.2 from, \circ , analytical simulation, \diamond , FE model, \square , experiment: the amplitude factor at Segment C is: (a)1, (b) 0.8, (c) 0.6, (d) 0.4, (e) 0.2, and (f) 0, respectively.

Table 1. Element quantity and crack size set-up for each case in FE simulations

Categories	Mesh element quantity				C.S.A.
	Pipe model	Crack			
		Arc length	Depth	Width	
Crack 1	1,214,468	42	4	2	4.17%
Crack 2	1,215,788	84	4	2	8.33%
Crack 3	1,217,140	126	4	2	12.50%

Table 2. Comparisons among analytical, FE predictions and test results for an array of transducers transmission depending on the reduced amplitude factor at segment C of the array

Amplitude Factor	Mean Absolute Percentage Error (%)		
	Analytical to FE Simulation	Analytical to Experiment	FE Simulation to Experiment
1.0	9.4142	5.4611	10.1632
0.8	9.882	6.2302	9.9138
0.6	8.3922	6.5832	3.6536
0.4	11.4122	10.5292	7.3153
0.2	15.7448	12.0432	7.006
0	19.4298	14.0483	6.2098